Available online at www.sciencedirect.com
SCIENCE DIRECT®
Journal of Constructional Steel Research 61 (2005) 587–606
JOURNAL OF CONSTRUCTIONAL STEEL RESEARCH
www.elsevier.com/locate/jcsr

Seismic behavior of steel beam and reinforced concrete column connections

Chin-Tung Cheng[a,*], Cheng-Chih Chen[b]

[a] *Department of Construction Engineering, National Kaohsiung First University of Science & Technology, 1 University Road, Yenchao, Kaohsiung 824, Taiwan*
[b] *Department of Civil Engineering, National Chiao Tung University, Hsinchu, Taiwan 300, Taiwan*

Received 7 May 2004; accepted 23 September 2004

Abstract

This paper aims to investigate the seismic behavior of steel beam to reinforced concrete column connections with or without the floor slab, acting as a proof test for a three-story–three-bay reinforced concrete column and steel beam (RCS) in-plane frame tested at the National Center for Research on Earthquake Engineering (NCREE), Taiwan, by the Taiwan–USA international research cooperation group. In total, six cruciform RCS joint sub-assemblages were constructed and tested. Parameters considered included composite effects of the slab and beam, the tie configuration in the panel zone, effects of the cross-beam, and the loading protocol. Force–deformation behavior was also simulated by a nonlinear analysis program, DRAIN-2DX, with consideration of composite effects of the beam and slab as well as shear distortion in the panel zone. Test results showed that all specimens performed in a ductile manner with plastic hinges formed in the beam ends near the column face. It was found that the ultimate strength of the composite beam was increased by 27% on average, compared with that of the steel beam without the slab.

Keywords: Composite structures; Beam–column connections; Panel zone

* Corresponding author. Tel.: +886 7 6011000x2118; fax: +886 7 6011017.
E-mail address: ctcheng@ccms.nkfust.edu.tw (C.-T. Cheng).

0143-974X/$ - see front matter © 2004 Elsevier Ltd. All rights reserved.
doi:10.1016/j.jcsr.2004.09.003

Notation

b_f	width of the beam flange
d_{beam}	depth of the steel beams
d_{pz}	depth of the panel zone
h_c	width of the column
f_c	concrete strength of the strut concrete in the panel zone
f'_c	concrete compressive strength
$(f_c)_{\text{eff}}$	effective concrete strength of the strut concrete in the panel zone
H	column height
I_{bp}	flexural inertia of the steel band plates
k_{tc}	ratio of the principal tensile and compressive strains of the strut concrete
k_c	parameter for considering the confinement of the strut concrete
k_{bp}	stiffness provided by the steel band plates
k_{pz}	total stiffness in the panel zone
k_{pzs}	stiffness provided by the panel shear only
L	beam length between two inflection points
L_{bp}	half-length of the steel band plates in the bending direction
t_w	width of the beam web
V_{ih}	shear strength resisted by the inner element of the panel zone
V_{oh}	shear strength resisted by the outer element of the panel zone
V_{wh}	shear strength resisted by the beam web in the panel zone
V_{pz}	total shear strength of the panel zone
Z	parameter for defining the post-peak descending slope in the stress–strain relation of the strut concrete
β	parameter for considering the softening effect of the concrete strength
ΔM	total beam end moment
ε_c	principal compressive strain of the strut concrete
ε_t	principal tensile strain of the strut concrete
ε_x	horizontal strain of the strut concrete
ε_y	vertical strain of the strut concrete
ε_o	concrete strain corresponding to f'_c
γ	shear strain in the panel zone
γ_{xy}	shear strain of the concrete in the panel zone
θ_p	angle of the diagonal strut corresponding to the beam flange
θ_{pz}	beam end rotation due to the panel shear

1. Introduction

Composite structures, including concrete filled steel tubes (CFT) and steel reinforced concrete (SRC) structures, have become popular in the US and Japan recently. One of the composite systems investigated, starting in 1989, is referred to as the RCS system. RCS composite systems resist seismic moments based on the connection between reinforced concrete columns and steel beams. Using RC rather than structural steel as columns can result in substantial savings in material cost and increase of the structural damping and lateral stiffness of the building. The two main categories in RCS connections to date can be characterized as the beam-through-type and the column-through-type. According to the literature, beams continuously passing through column panel zones (beam-through-type) behave in a ductile manner under seismic loading; however, orthogonal moment connection in the panel zone may be labor intensive. Use of the column-through-type, using diaphragms or cover plates to connect the steel beam and column, may facilitate field construction; however, additional effort in connection details to ensure a better seismic capacity in terms of strength and ductility is needed.

In 1989, Deierlein et al. [1] and Sheikh et al. [2] started the research on RCS composite systems in Texas University, where 15 beam-through-type connections without slabs were tested. Two distinct failure modes in RCS systems were identified: panel zone yielding and bearing failure of column concrete when subjected to cyclic loading, as shown in Fig. 1. In 1993, Kanno [3] tested a series of RCS connections without the slab. Research parameters included tie details in the panel zone, the column axial load, and the bearing strength of the concrete. Test results showed that the seismic capacity of RCS systems was not less than that of reinforced concrete or steel structures. Since 1997, cooperative research on RCS systems has been conducted in the US and Japan, such as the work of Baba and Nishimura [4], Kim and Noguchi [5], Nishiyama et al. [6], Parra-Montesinos and Wight [7], and Bugeja et al. [8].

To study the composite effects of the steel beam and floor slab, Yu et al. [9] have tested several composite beam to steel or SRC column connections. Test results showed that composite effects may vary with the types of connection, distribution of shear studs, slab thickness, and amount of reinforcing bars in the slab. In general, the shallow beam depth used in low rise to mid-rise buildings tends to have larger composite effects. Test results also revealed that slabs provided lateral support for the beam top flange, preventing torsional buckling. In addition, floor concrete also increased the flexural stiffness for the composite beams. Beside this research, Liu and Astaneh-Asl [10] also conducted six tests of composite beam to steel or RC column connections. Investigated parameters included connection details, shear studs, and the slab reinforcement. Test results showed that the composite effect was sustained until the drift angle reached 0.04 rad.

In 2002, a Taiwan–US research cooperation group proposed to test a full-scale three-story–three-bay in-plane RCS frame. Before the frame test, the seismic behavior of the beam–column connections needs to be clarified. According to the literature, beam-through-type connections may have improved seismic performance when compared with the column-through-type ones. Therefore, six full-scale beam-through-type composite beam–column sub-structures were designed and tested, to act as a component test for the design of a three-story–three-bay in-plane RCS frame. Parameters considered included

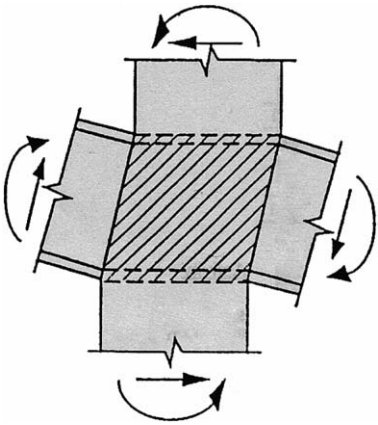

(a) Panel shear failure.

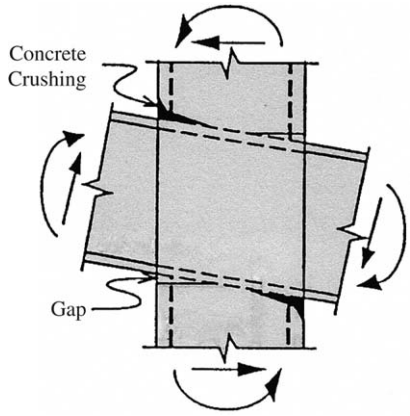

(b) Bearing failure.

Fig. 1. The failure mechanism of an inner panel [3].

composite effects of the slab, tie details in the panel zone, effects of the transverse beam, and the loading protocol.

2. Experiments

In the full-scale plane frame, the span of the columns was seven metres from centerline to centerline of the columns with four metres of story height. Based on loading combinations, the beam sections from the roof to the first floor were designed to be $H396 \times 199 \times 7 \times 11$, $H500 \times 200 \times 10 \times 16$, and $H596 \times 199 \times 10 \times 15$. In the sub-structural tests, as shown in Figs. 2 and 3, all specimens have the same dimensions, with the steel beam $H596 \times 199 \times 10 \times 15$ in size and 65×65 cm columns reinforced with 12 #11 longitudinal bars, representing beam–column connections of the first floor of the in-plane frame. According to the research of Kanno and Deierlein [11], the panel

Fig. 2. A photograph showing specimen ICLCS before the test.

zone of beam-through-type connections can be divided into two elements: inner and outer elements. Failure modes in the inner element can be panel shear yielding or bearing failure of the column concrete, while failure modes in the outer element may be bond failure of the longitudinal reinforcement or panel shear yielding. To prevent these premature failures for all specimens, two retrofit techniques were applied, as shown in Fig. 4. To prevent bearing failure of the column concrete that faces the steel beam, band plates (BP) were embedded around the column. To enhance the shear transfer in the panel zone, face-bearing plates (FBP) were fillet welded to the beams at the column face.

In the labeling of the six specimens, the first character, I, represents the interior column connections. The second character, C or N, represents whether the connection is with or without a cross-beam in the orthogonal direction, respectively. The third character represents the shape of the ties reinforced in the panel zone. As shown in Fig. 5, L-shaped, square, and U-shaped ties were used in the specimens with or without a cross-beam intersected in the panel zone. The fourth character distinguishes different loading protocols, with C for cyclic loading and P representing near-fault pulse-type loading. If a fifth character S is added, it indicates a composite beam with a steel beam supporting a reinforced concrete slab on a metal deck, these acting together to resist bending through the shear studs. Fig. 6 shows the distribution of shear studs on the beam, and the temporary brace for the pouring of the floor concrete. As shown in the figure, the slab was reinforced with #3 bars spaced 300 mm apart in the bottom layer and wire mesh 7 $\varphi \times 7$ φ mm with 100×100 mm spacing in the upper layer. The material strengths of steel are summarized in Table 1. Table 2 shows the compressive strength of the concrete. As shown in Fig. 3, the column with shorter beams was precast together at the factory for easy transportation and

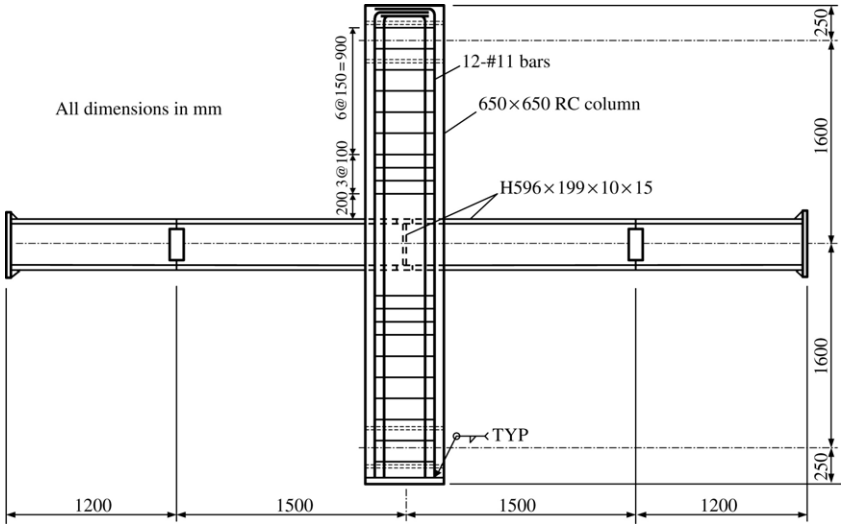

Fig. 3. Details of the beam–column joint.

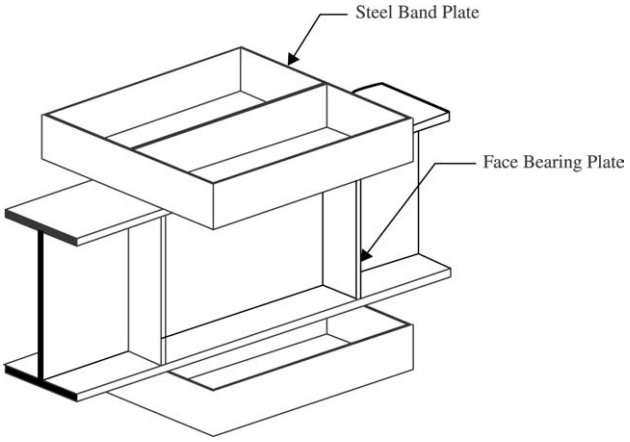

Fig. 4. Two reinforcing techniques in the panel zone of the beam-through-type connections.

then spliced with extended beams using bolts in the laboratory. Specimen ICLC was the first one to be tested; however, slips at the beam splice that occurred during testing caused a sudden drop in the force–deformation curve. Therefore, the splice plates were fillet welded to the beam to prevent slips for the remaining tests.

Fig. 7 shows the test apparatus. Before the test, the hydraulic jack at the top of the column applied a 1000 kN constant axial load to represent the gravity load that was obtained from the frame analysis. Then hydraulic actuators at each beam tip applied the cyclic load with displacement control in the form of triangular waves, as shown in Fig. 8. During the test, a horizontal actuator at the top of the column held the column in

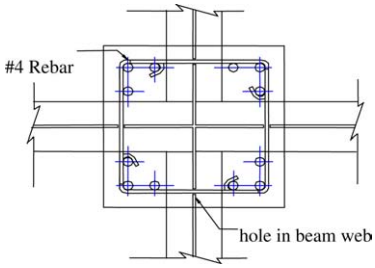

(a) Four L-shaped ties.

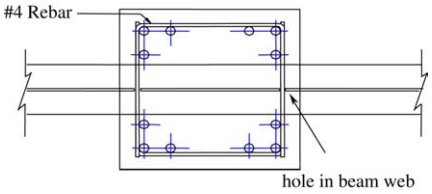

(b) Two U-shaped ties.

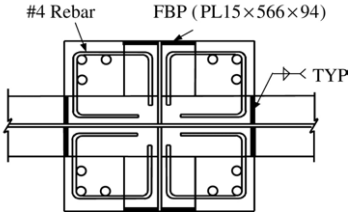

(c) Four square ties.

Fig. 5. Shapes of ties in the panel zone.

Table 1
Material strength for the steel

Item	Rebar #3	Rebar #4	Rebar #11	Beam web	Beam flange
f_y (N/mm^2)	442.3	430.7	443.3	478.5	444.2
f_u (N/mm^2)	650.3	680.6	674.6	598.7	568.0

Table 2
Concrete strength

Specimen	Column f'_c (N/mm^2)	Slab f'_c (N/mm^2)
ICLCS	48.9	22.5
INUCS	54.5	24.3
ICLPS	49.9	21.0
ICLC	52.4	–
ICSC	42.7	–
INUC	54.3	–

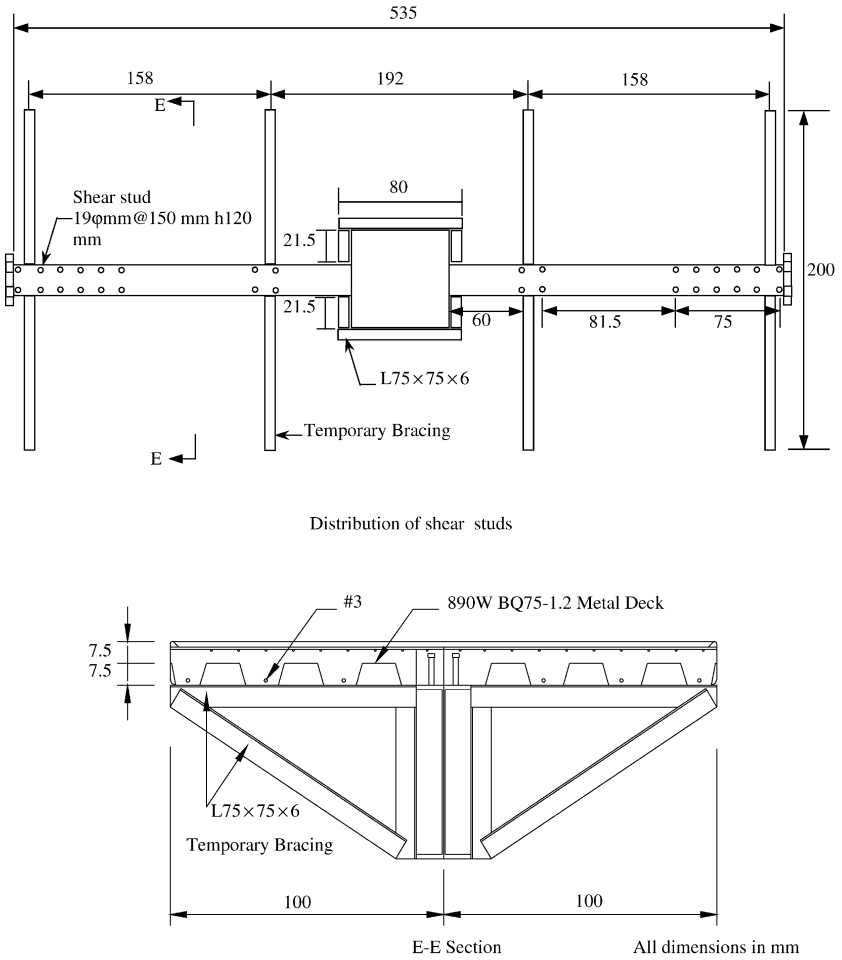

Fig. 6. Details of the composite beam.

position, but allowed it to rotate accordingly. For specimen ICLPS, the loading protocol simulates the waveform of near-fault excitations, as shown in Fig. 9, based on the report of Krawinkler et al. [12].

The test results show that all specimens performed in a ductile manner with plastic hinges formed at the beam ends near the column face, where local buckling took place successively at the beam flange and web, and only minor damage such as cracks was observed in the column and the panel zone. Visual observation revealed that all specimens except ICLPS performed similarly, with yielding and local buckling of the beam bottom flange occurring at drifts of 1.0% and 4.0%, respectively. For specimens with a slab, the composite effect disappeared after 3% drift because of the insufficient shear transfer provided by the shear studs which were fractured during the test. With the lateral support of the floor slab, the beam top flange can only buckle downward at 5.0% drift, compared

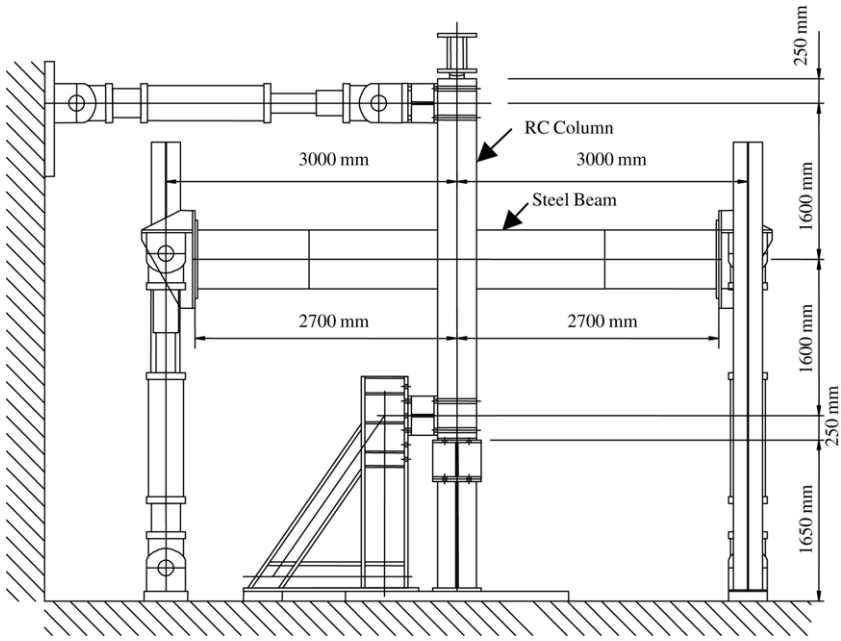

Fig. 7. Test apparatus.

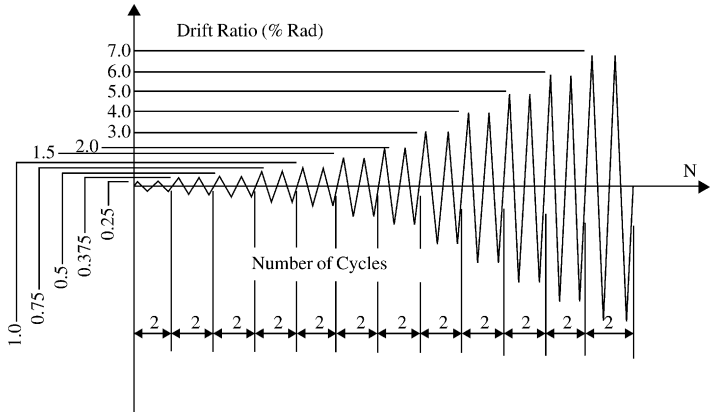

Fig. 8. The loading protocol for all specimens except ICLPS.

with 4.0% drift for the specimens without a slab. All tests concluded at the drift of 6% due to the fracture of the beam bottom flange—with the exception of that for specimen INUC, which fractured in the top flange. Figs. 10 and 11 show images at the conclusion of testing for specimens INUCS and INUC, respectively. For specimen ICLPS loaded with the near-fault protocol, fracture of the bottom flange and separation of the beam and the slab was not seen till the end of the testing, unlike in the tests of specimens INUCS and ICLCS. Since all connections were designed and behaved in a strong column and weak

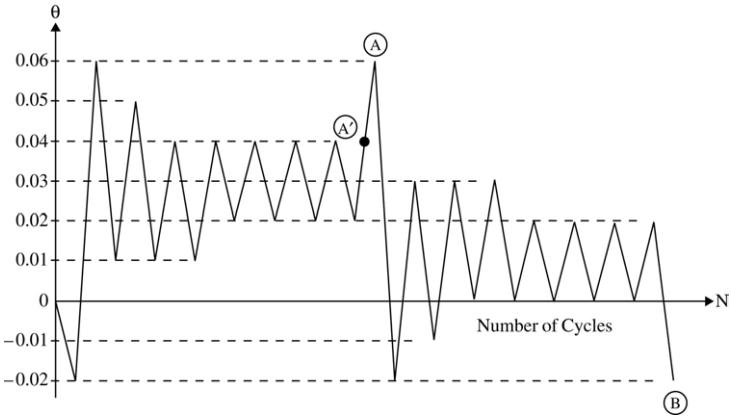

Fig. 9. The loading protocol for specimen ICLPS [12].

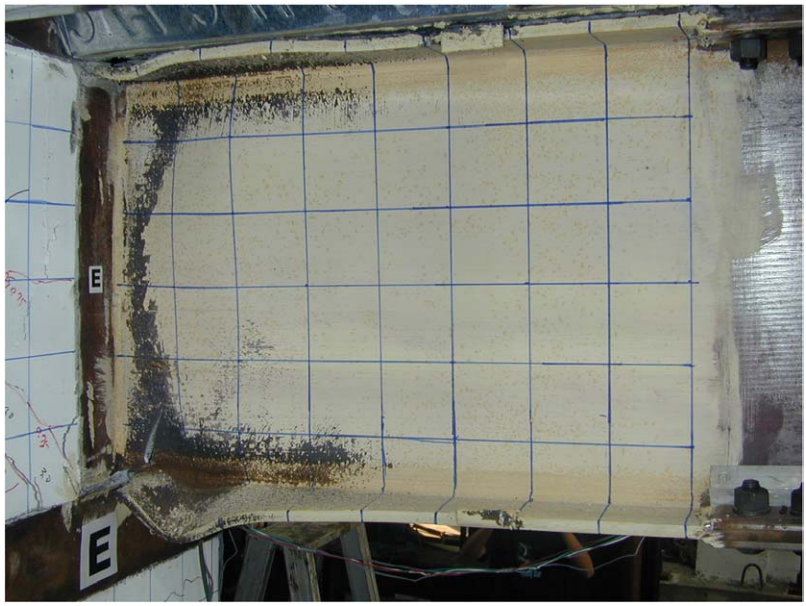

Fig. 10. A photograph showing the fracture of the beam flange for specimen INUCS after the test.

beam manner with the column and panel zone remaining elastic at all times, the factor of the cross-beam and the configuration of the ties in the panel zone had only a marginal effect on the seismic performance.

Fig. 12 shows the hysteretic curves of force versus displacement at the east beam end for all specimens. On the basis of these figures, the ultimate strength and initial stiffness of each specimen under positive and negative bending were obtained, and these are summarized in Table 3. Under positive bending, it was found that the initial stiffness

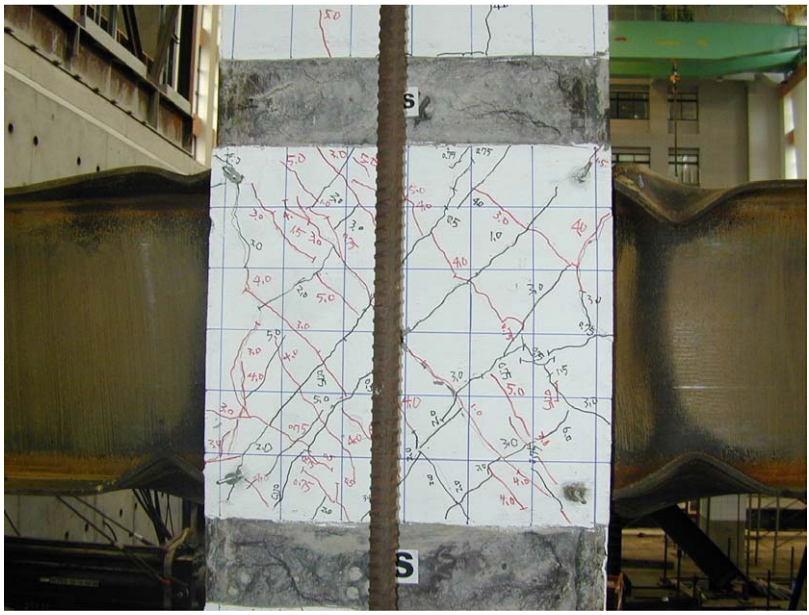

Fig. 11. A photograph showing the damage of the beam flange for specimen INUC after the test.

Table 3
The strength and stiffness of the specimens

Specimens	Experimental results							Analytical panel shear (kN)		
	Moment in east Beam (kN m)		Moment in west Beam (kN m)		Stiffness (kN/m)		Panel Shear (kN)	K & D	P & W	AIJ
	Positive	Negative	Positive	Negative	Positive	Negative				
ICLCS	1539	1283	1609	1236	17592	10643	3884	3440	5557	5671
INUCS	1701	1342	1652	1337	17571	12257	4134	3572	5760	5790
ICLPS	1669	1218	1661	1307	14999	10666	4012	3458	5746	5694
ICLC	1286	1256	1274	1229	10883	10463	3457	3527	5935	5749
INUC	1293	1276	1275	1229	12321	11515	3477	3570	5760	5546
ICSC	1272	1253	1244	1204	12418	10776	3408	3229	5083	5788

and ultimate strength of the composite beams increased by 67% and 27% on average, respectively, when compared to those for the steel beam without a slab. Under negative bending, the average ultimate strength of specimens with a slab is 1.02 times that of specimens without a slab. It is also noted that the post-peak deterioration of specimen ICLPS is less than that of other specimens due to the different loading protocol. Table 3 also summarizes the analytical shear strength in the panel zone, based on the research of Kanno and Deierlein [11], Para-Montesinos and Wight [7], and AIJ [13]. It was found that Kanno and Deierlein's suggestions tend to be conservative for the design of connections, when compared with the test results.

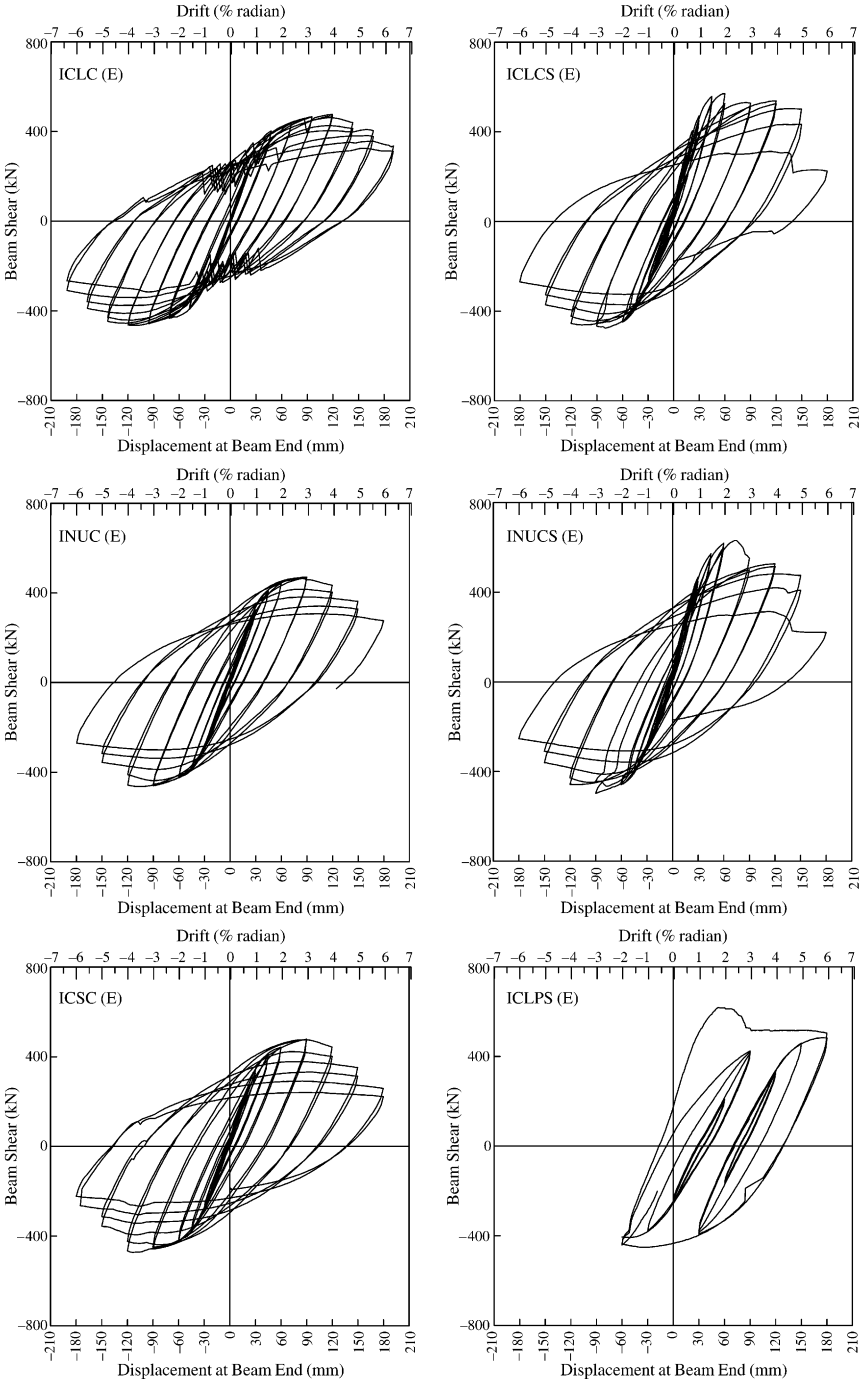

Fig. 12. Hysteretic curves for the specimens.

On the basis of the measurements made using transducers and inclinometers installed in the joint area, beam end deformations can be decomposed into components due to the flexural deflection of the column and the beam, in addition to the shear distortions in the panel zone. Panel zone deformations consist of distortions due to the panel shear and the concrete bearing. Fig. 13 shows a typical decomposition of deformations for specimen ICLCS. As shown in this figure, most of the nonlinear deformations were concentrated on the beam, while the flexural deformation of the column and distortion due to the concrete bearing in the panel zone remained elastic at all times, and a slightly inelastic distortion was induced by the joint shear.

3. Force–deformation simulations

The DRAIN-2DX program [15] was applied to simulate the force–deformation behavior of RCS beam–column connections. This program can simulate the nonlinear behavior of the beam and column easily upon inputting its material properties and failure surface, while a simulation of the inelastic deformation of the panel zone needs to be created. As shown in Fig. 13, panel zone deformations consist of distortions due to the bearing of the column concrete and panel shear. According to the research of Para-Montesinos and Wight [7], panel shear can be resisted by the superposition of three components such as the concrete struts in the inner and outer elements, and the steel beam web. Compatibility in this disturbed region suggests that

$$\varepsilon_c = \frac{\varepsilon_x + \varepsilon_y}{2} + \frac{\varepsilon_x - \varepsilon_y}{2}\cos(2\theta_p) + \frac{\gamma_{xy}}{2}\sin(2\theta_p) \tag{1}$$

$$\varepsilon_t = \frac{\varepsilon_x + \varepsilon_y}{2} + \frac{\varepsilon_x - \varepsilon_y}{2}\cos[2(\theta_p + 90^\circ)] + \frac{\gamma_{xy}}{2}\sin[2(\theta_p + 90^\circ)] \tag{2}$$

where $\gamma_{xy} = \tan(2\theta_p)(\varepsilon_x - \varepsilon_y)$, ε_c and ε_t are the principal compressive and tensile strains of the concrete strut, ε_x and ε_y are the horizontal and vertical strains of concrete strut, and θ_p is the main concrete strut angle. On the basis of the geometry, the strut angles for the inner and outer elements can be shown to be as follows:

$$\theta_{\text{inner}} = a\tan\left(\frac{d_{\text{beam}}}{h_c}\right) \tag{3}$$

$$\theta_{\text{outer}} = a\tan\left(\frac{1.25d_{\text{beam}}}{h_c}\right) \tag{4}$$

where d_{beam} is the depth of the steel beams and h_c is the width of the column. Empirical values of $k_{tc} = -\varepsilon_t/\varepsilon_c$, varying with different details such as 'T-shaped' or cruciform joints, and inner or outer elements, are provided in the paper of Para-Montesinos and Wight [7]. By using Eqs. (1)–(4), and the k_{tc} value, the shear strain γ_{xy} and ε_c can be obtained.

For the inner element, the stress–strain relationship of the strut concrete can be expressed as

$$f_c(\varepsilon_c) = f'_c[2(\varepsilon_c/\varepsilon_0) - (\varepsilon_c/\varepsilon_0)^2] \qquad \varepsilon_c \le \varepsilon_0 \tag{5}$$

$$f_c(\varepsilon_c) = f'_c[1 - Z(\varepsilon_c - \varepsilon_0)] \qquad \varepsilon_c > \varepsilon_0 \tag{6}$$

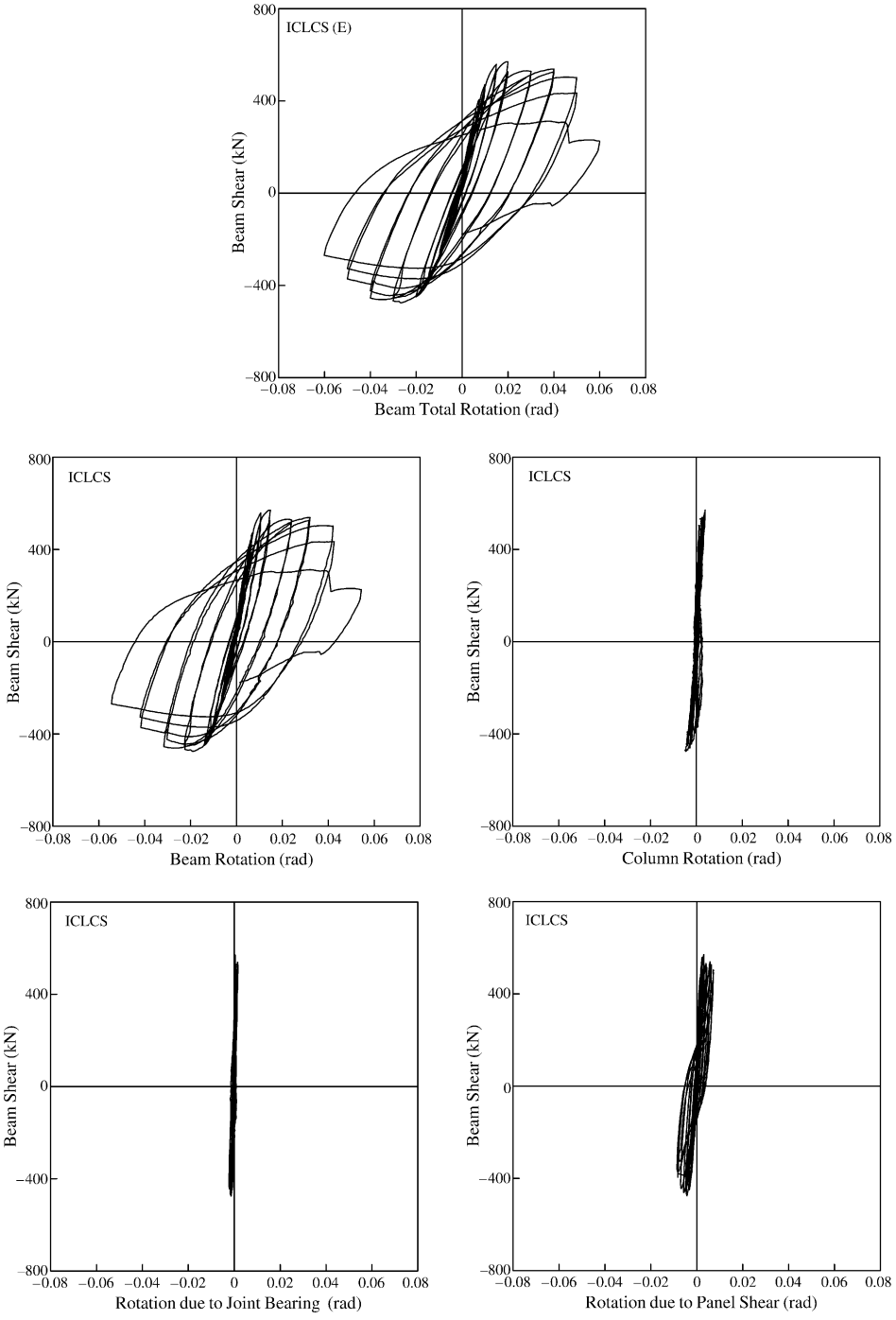

Fig. 13. The displacement decoupling for specimen ICLCS.

where f_c' is the concrete compressive strength (N/mm^2), ε_c is the concrete strain corresponding to f_c, ε_0 is the concrete strain corresponding to f_c', and Z is the parameter for defining the post-peak slope of descending strength. Z is 50 for the inner element and

$$\varepsilon_0 = 0.001648 + 0.0000165 f_c'. \tag{7}$$

Therefore, the effective strut concrete stress is expressed as

$$(f_c)_{\text{eff}} = f_c(\varepsilon_c) k_c \beta \tag{8}$$

where k_c takes into consideration the confinement of the concrete. In general, k_c is equal to 2.0. If a cross-beam intersects in the panel zone, k_c is equal to 2.3. β takes into consideration the softening effect on the concrete strength due to the orthogonal tension in the panel zone. According to the research of Vecchio and Collins [14], β is

$$\beta = \frac{1}{0.85 - 0.27\frac{\varepsilon_t}{\varepsilon_c}} = \frac{1}{0.85 + 0.27 k_{tc}} \tag{9}$$

where k_{tc} is the ratio of the principal tensile and compressive strains of the concrete strut. Then, the shear strength resisted by the inner element is

$$V_{ih} = 0.3(f_c)_{\text{eff}} h_c (b_f - t_w) \tag{10}$$

where h_c is the column width, b_f is the width of the beam flange, and t_w is the width of the beam web.

The calculation of the shear strength resisted by the outer element is the same as that for the inner element except for the adjustments of the parameters Z, β, and k_c. When ties are applied in the panel zone, k_c is equal to 1.1. Application of steel band plates in addition to ties increases k_c to 1.5. If steel band plates are applied alone without ties, k_c is adjusted to 1.3. Under the above conditions, Z is equal to 150. If steel plates are applied to confine the panel zone, k_c is equal to 2.0 for the inner and outer elements, and Z is equal to 50. Therefore, the shear strength resisted by the outer element is calculated as

$$V_{oh} = 0.3(f_c)_{\text{eff}} h_c b_0 \tag{11}$$

where b_0 is the effective width of the outer element defined in the research of Para-Montesinos and Wight [7]. The shear strength resisted by the beam web can be calculated as

$$V_{wh} = \int_0^{h_c} \tau_{\text{web}}(x) t_w \, \mathrm{d}x \tag{12}$$

where $\tau_{\text{web}}(x) = \gamma_{\text{web}}(x) G_s \le \frac{f_y}{\sqrt{3}} = \tau_y$. Then, the shear strength of the panel zone is the superposition of three components:

$$V_{pz} = V_{ih} + V_{oh} + V_{wh}. \tag{13}$$

Fig. 14 shows the shear force–strain curve predicted using this model together with results from experiments on the specified specimens. The prediction was calculated on the basis of 42 N/mm^2 concrete strength and 420 N/mm^2 yield strength for the steel. It was found that the predictions might have higher stiffness than the tests. The reason is that this analysis did not account for the distortion of the band plates that were applied to prevent

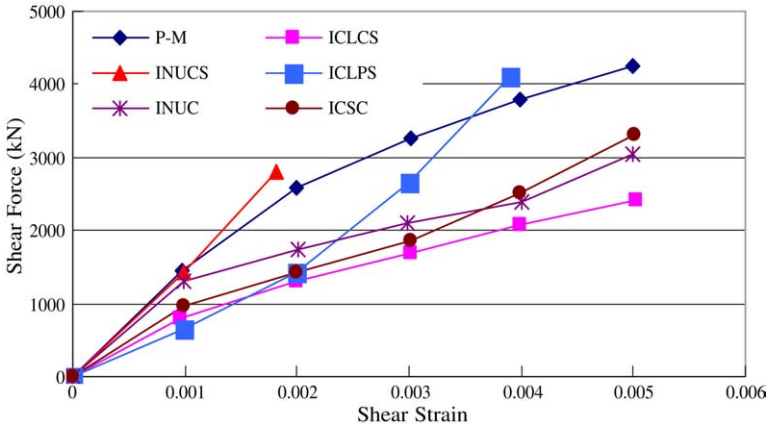

Fig. 14. The panel shear force and strain relationship predicted by the theory of Parra-Montesinos [7].

the bearing failure of the column concrete. Therefore, the stiffness of the band plates can be estimated using

$$k_{bp} = 3E_s I_{bp}/L_{bp}^3 \tag{14}$$

where I_{bp} is the second moment of area of the three plates and L_{bp} is the half-length of the band plates as shown in the Fig. 4. Fig. 15 shows that the analytical stiffness may be appropriate when compared with the tests. Therefore, the total stiffnesses of the panel zone k_{pz} due to the concrete bearing and panel shear may be combined and expressed as

$$1/k_{pz} = 1/k_{bp} + 1/k_{pzs} \tag{15}$$

where k_{pzs} is the shear stiffness, as shown in Fig. 14. Fig. 16 shows the comparison between the total panel stiffness predicted and the test results. It is found that the proposed prediction is more appropriate than the prediction shown in Fig. 14.

To simulate the force–deformation behavior of beam–column connections by using DRAIN-2DX, the panel shear distortion can be applied to replace the rigid joint. However, this shear force–strain relationship needs to be transformed into a moment–rotation relationship due to the loads applied at the beam tip in the tests, as shown in Fig. 17. The beam end total moments ΔM and panel shear V_{pz} can be related as

$$V_{pz} = \frac{\Delta M}{d_{pz}}\left(1 - \frac{d_{pz}L}{H(L-h_c)}\right) \tag{16}$$

where d_{pz} is the depth of the panel zone, L is the beam length between two inflection points (actuators), H is the column height between two inflection points, and h_c is the column width. The beam end rotations due to panel shear, θ_{pz}, and shear strain in the panel zone, γ, can be related as

$$\theta_{pz} = \gamma\left[1 - \frac{d_{pz}L}{H(L-h_c)}\right]. \tag{17}$$

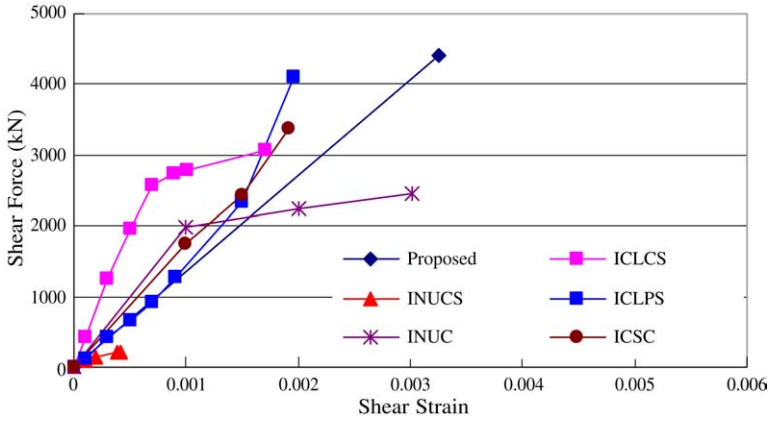

Fig. 15. The shear force and strain relationship due to the bearing.

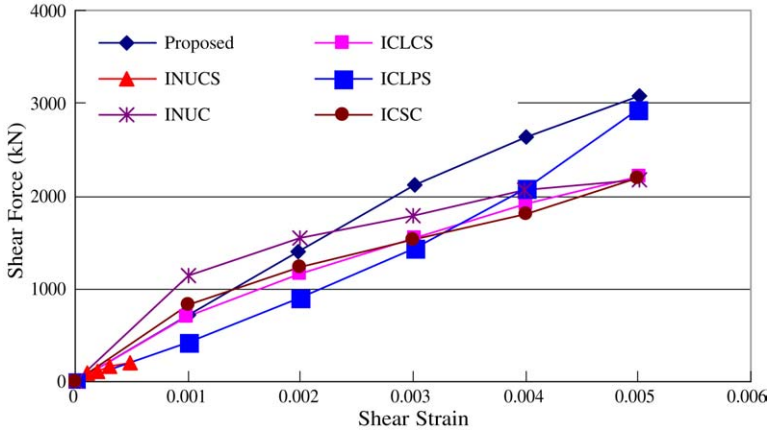

Fig. 16. The proposed shear force and strain relationship due to the bearing and panel shear.

According to Eqs. (16) and (17), the panel shear force and strain relationship of the joints can be transformed into a beam end moment and rotation relationship in the form of four springs, as shown in Fig. 17. The four nodal points within the rotational springs have the same coordinate slaving together. This model was built to simulate the force–deformation behavior of an east beam subjected to the load at the beam tip by the vertical actuator. Therefore, the boundary condition on the inflection points was set the same as for the test apparatus for the specimens.

Fig. 17 also shows a compression link element for compensating for the composite effect due to the floor slab that only exists when the beam is subjected to positive bending. On the basis of AISC-LRFD provisions [16], the stiffness of the link elements was calculated as the difference of the bare steel beam effect without the slab and the composite effect of the steel beam with the slab, and transformed into the direction of the link element.

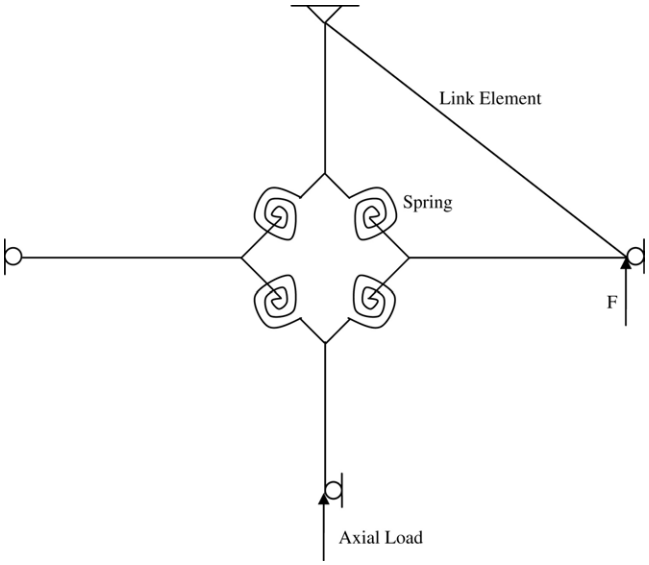

Fig. 17. A schematic graph showing a model of the beam–column sub-structure.

A tri-linear force–deformation relationship for simulating the behavior of the slab concrete was adopted for the link element. The bare steel beams were modeled by a beam–column element with a bi-linear force–deformation relationship acting in an elastic–plastic manner. The yield strength was calculated on the basis of the plastic modulus of the steel beam section. The ratio of the post-yield stiffness to the initial stiffness was set to be 0.01 to account for the strain-hardening effect of the steel. The reinforced concrete columns were also modeled by a beam–column element with a yield surface based on the interaction between the axial load and the moment applied on the columns. For the column stiffness, an effective second moment of area (70%) was used to account for the flexural cracks. Finally, monotonic loads were applied on the beam tip to simulate the experimental procedure. Fig. 18 shows the predictions for the force–deformation relationship compared with test results for the specimens ICLCS and ICLC. It is found that the force–deformation simulations agree very well with test results for both specimens.

4. Conclusions

Test results show that all specimens performed in a ductile manner with plastic hinges formed in the beam ends near the column face. Under positive bending, it was found that the initial stiffness and ultimate strength of the composite beam had average increases of 67% and 27% respectively, compared with the steel beam without the slab. Under negative bending, similar ultimate strengths of specimens with and without the slab were obtained. This composite action disappeared after 3% drift of loading and then the lateral strength slowly deteriorated until fracture of the bottom flange occurred. Sub-structure loaded by a near-fault protocol performed well, showing good strength and ductility, slightly better than

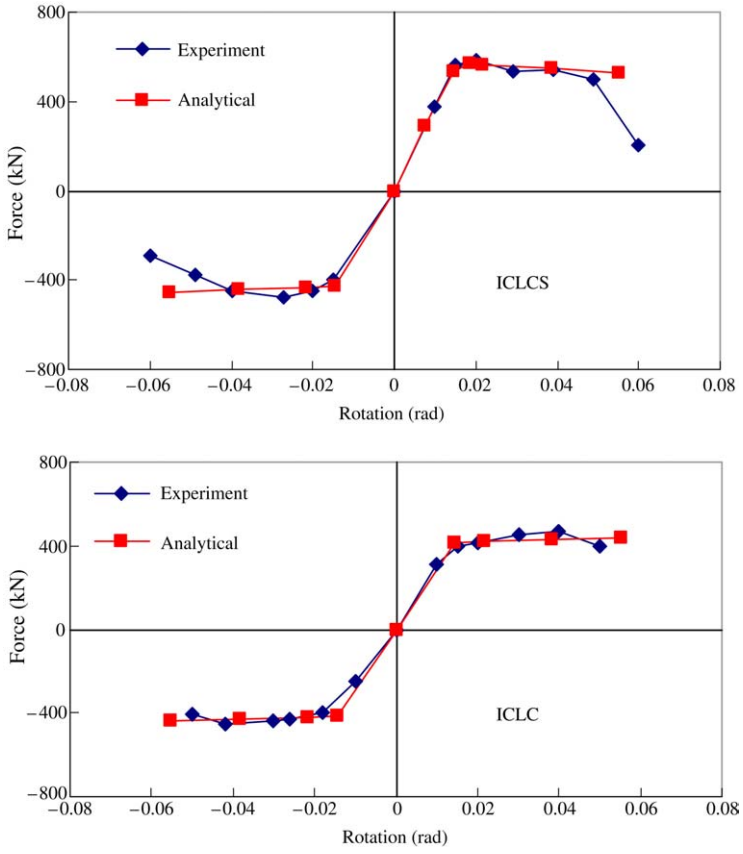

Fig. 18. Predicted force–deformation relationships for specimens ICLCS and ICLC.

that of other tests where fracture of the bottom flange and separation of the beam and the slab was seen during the test. Moreover, the test performance revealed that cross-beams and the configuration of ties in the panel zone had only a marginal effect on the shear transfer in the panel zone due to the strong column and weak beam design for all specimens.

On the basis of the comparison of the force–deformation simulation and test results, it was found that distortions in the panel zone accounting for the concrete bearing in addition to the panel shear can appropriately predict the total shear stiffness in the panel zone of RCS connections. Adding a compression link element to simulate the composite effect of the slab, the DRAIN-2DX program can simulate the envelope of the force–deformation relation for composite RCS beam–column sub-structures.

Acknowledgements

Financial support from the National Science Council in Taiwan and technical help from the NCREE Labs are greatly appreciated. The authors would also like to thank Mr. P.H. Chan, J.T. Yang and N.J. Lin for their assistance in the experiment.

References

[1] Deierlein GG, Sheikh TM, Yura JA, Jirsa JO. Beam–column moment connections for composite frames: part 2. Journal of Structural Engineering, ASCE 1989;115(11):2877–96.
[2] Sheikh TM, Deierlein GG, Yura JA, Jirsa JO. Beam–column moment connections for composite frames: part 1. Journal of Structural Engineering, ASCE 1989;115(11):2858–76.
[3] Kanno R. Strength deformation, and seismic resistance of joints between steel beams and reinforced concrete columns. Ph.D. dissertation, Cornell University, Ithaca, NY; 1993.
[4] Baba N, Nishimura Y. Stress transfer on through beam type steel beam-reinforced concrete column joints. In: Proc. of 6th ASCCS conference. 2000. p. 753–60.
[5] Kim K, Noguchi H. An analytical study on the shear strength of RCS joints. In: 4th JTCC meeting. 1997.
[6] Nishiyama I, Itadani H, Sugihiro K. 3D beam–column connection (joint panel) tests on RCS. In: 4th JTCC meeting. 1997.
[7] Parra-Montesinos G, Wight JK. Seismic response of exterior RC column-to-steel beam connections. Journal of Structural Engineering, ASCE 2000;126(10):1113–21.
[8] Bugeja MN, Bracci JM, Moore WP. Seismic behavior of composite RCS frame systems. Journal of Structural Engineering, ASCE 2000;126(4):429–36.
[9] Yu QS, Noel S, Uang CM. Composite slab effects on strength and stability of moment connections with RBS or welded haunch modification. In: Proc. of 6th ASCCS conference. 2000. p. 705–12.
[10] Liu J, Astaneh-Asl A. Cyclic behavior of shear connections with floor slab. In: Proc. of 6th ASCCS conference. 2000. p. 745–52.
[11] Kanno R, Deierlein GG. Design model of joints for RCS frames. In: Composite construction in steel and concrete IV. ASCE; 2000.
[12] Krawinkler H, Gupta A, Medina R, Luco N. Development of loading histories for testing of steel beam–column assemblies. Report for the SAC steel project by FEMA; 2000.
[13] AIJ composite committee. Design guidelines for composite RCS joints. Tokyo: Architectural Institute of Japan; 1994.
[14] Vecchio FJ, Collins MP. Compression response of cracked reinforced concrete. Journal of Structural Engineering, ASCE 1993;119(12):3590–610.
[15] Prakash V, Powell GH. DRAIN-2DX user guide. Department of Civil Engineering, University of California at Berkeley; 1992.
[16] American institute of steel construction (AISC). Manual of steel construction load and resistance factor design (LRFD). 3rd ed. Chicago (IL): AISC; 2001.